Applied Computing and Geosciences 19 (2023) 100129

Contents lists available at ScienceDirect

Applied Computing and Geosciences

journal homepage: www.sciencedirect.com/journal/applied-computing-and-geosciences

Python programs to apply regularized derivatives in the magnetic tilt derivative and gradient intensity data processing: A graphical procedure to choose the regularization parameter

Janaína Anjos Melo *, Carlos Alberto Mendonça, Yara Regina Marangoni

University of São Paulo, Department of Geophysics, Rua do Matão, 1226, São Paulo, 05508-090, SP, Brazil

ARTICLE INFO

Keywords:
Regularized derivative
Aeromagnetic data
Regularization parameter
Staircase function

ABSTRACT

The Tikhonov regularization parameter is a key parameter controlling the smoothness degree and oscillations of a regularized unknown solution. Usual methods to determine a proper parameter (L-curve or the discrepancy principle, for example) are not readily applicable to the evaluation of regularized derivatives, since this formulation does not make explicit a set of model parameters that are necessary to implement these methods. We develop a procedure for the determination of the regularization parameter based on the graphical construction of a characteristic "staircase" function associated with the L_2-norm of the regularized derivatives for a set of trial regularization parameters. This function is independent of model parameters and presents a smooth and monotonic variation. The regularization parameters at the upper step (low values) of the ''staircase'' function provide equivalent results to the non-regularized derivative, the parameters at the lower step (high values) leading to over-smoothed derivatives. For the evaluated data sets, the proper regularization parameter is located in the slope connecting these two flat end-members of the staircase curve, thus balancing noise amplification against the amplitude loss in the transformed fields. A set of Python programs are presented to evaluate the regularization procedure in a well-known synthetic model composed of multiple (bulk and elongated) magnetic sources. This numerical approach also is applied in gridded aeromagnetic data covering high-grade metamorphic terrains of the Anápolis-Itauçu Complex in the Brasília Fold Belt central portion of Tocantins Province, central Brazil, characterized by multiple magnetic lineaments with different directions and intersections which are associated with shear zones, geologic faults, and intrusive bodies. The results obtained from the regularization procedure show efficiency in improving the maps of filtered fields, better tracking the continuity of magnetic lineaments and general geological trends. The results from the application in the Brasília Fold Belt enhance the importance and broader coverage of the Pirineus Zone of High Strain.

1. Introduction

The evaluation of first or higher-order derivatives for potential field data occupies a key processing stage in most modern crustal studies and mineral exploration projects using airborne magnetic data. Derivatives are used to enhance subtle anomaly variations from deeper or low-contrasting sources and are the base for automatic approaches using gradient fields. Two examples of these methods are the 3D analytical signal amplitude (ASA) (Roest et al., 1992) and its associated tilt derivative (TDR) (Miller and Singh, 1994). The ASA maxima tend to be located on the top of thin magnetic bodies or in the contact of contrasting magnetic structures. ASA and TDR are effective as edge detectors, a variety of tilt angles methods with first or higher-order derivatives better discriminating contributions from shallow and deep sources. Some examples of these angle-based edge detectors are known as total horizontal gradient of TDR (Verduzco et al., 2004), theta map method (Wijns et al., 2005), normalized horizontal tilt angle (Cooper and Cowan, 2006), horizontal gradient tilt angle (Ferreira et al., 2013), tilt angle of the first-order vertical derivative of the total horizontal gradient (Zhang et al., 2014), tilt angle of the ratio between the first-order horizontal gradient and the second-order horizontal gradient of the anomaly (Ma et al., 2014), tilt angle of the ASA (Cooper, 2014), ratio of the vertical derivative to the total horizontal derivative of the ASA (Pham et al., 2019).

* Corresponding author.
E-mail addresses: janaina.melo@usp.br (J.A. Melo), carlos.mendonca@iag.usp.br (C.A. Mendonça), yaramaran@usp.br (Y.R. Marangoni).

https://doi.org/10.1016/j.acags.2023.100129
Received 27 March 2023; Received in revised form 19 June 2023; Accepted 21 June 2023
Available online 28 June 2023

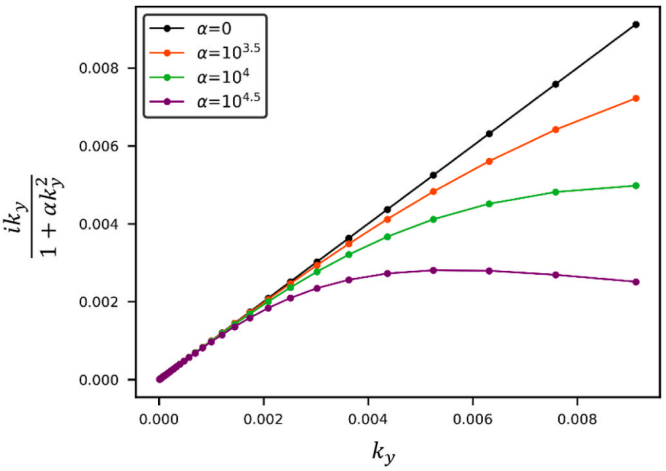

Fig. 1. Power spectrum of regularized y-derivative as a function of wavenumber for different regularization parameters. The $\alpha = 0$ condition represents the true filter derivative (black line), a situation in which no regularization is applied.

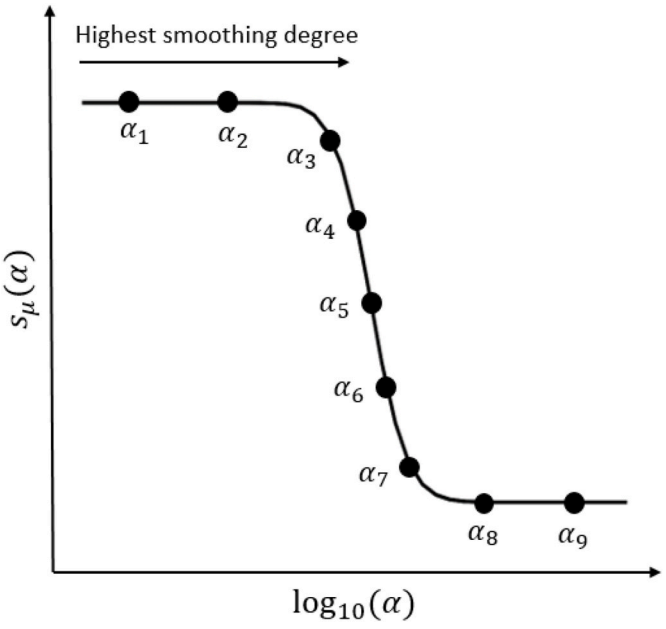

Fig. 2. Generic form of the S-function for variable trial regularization parameters $\alpha_1 < \alpha_2 < ... < \alpha_9$, the ending term α_1 represents a non-regularized derivative with oscillations, the α_9 over-smooths the derivatives with enhanced amplitude loss. Middle slope parameters, α_4 to α_6, better featuring smooth derivatives.

When processing large aeromagnetic databases, the calculation of horizontal and vertical derivatives of potential fields is usually performed in the Fourier domain (Blakely, 1996, p. 324). This kind of operation tends to amplify the noisy high-frequency spectral content in the observed data. To overcome this noise-enhancing problem, Pašteka and Richter (2002) and Richter and Pašteka (2003) developed the concept of regularized derivatives in the Fourier domain based on Tikhonov's regularization theory (Tikhonov and Glasko, 1965). The mathematical development of this approach was summarized by Pašteka et al. (2009), the regularized derivative is implemented as a low-pass filter, derived from minimizing the L_2-norm of the wished derivative, while balancing its smoothness degree with oscillations from noise amplification. The smoothness degree is linked to the choice of the regularization parameter, which as suggested by Pašteka et al. (2009), can be determined by tracking the variation of the anomaly-derivative amplitude for increasing trial regularization parameters, a possible "optimum" parameter set as the amplitude variation is minor, or below a threshold level. For a complex real data set, this criterion may generate multiple points of minima, preventing a clear choice for a specific regularization parameter. Common procedures based on the L-curve (Hansen, 1994, 1998) or the discrepancy principle (Morozov, 1966; Aster et al., 2013), for example, are not readily applicable to the regularized derivatives in the Fourier domain since this formulation does not make explicit a set of model parameters, which are necessary to implement these methods.

In processing gridded magnetic data, a good choice for the regularization parameter should provide processing products with minor distortions from noise amplification from unlevelled flight lines or spurious "eye-bull" features along lineaments with gentle amplitude variation. We present a new procedure for the determination of the regularization parameter based on the construction of a characteristic "staircase" function, relating to the L_2-norm of the anomaly-derivative for a set of trial regularization parameters. The regularization parameters in the upper step (low trial regularization values) of this smooth and monotonic function give equivalent results to the non-regularized derivative, meanwhile over-smoothing the derivatives for regularization parameters at the lower step (high trial values). Regularization parameters better balancing noise amplification with respect to amplitude loss are set at the slope connecting these two flat end-members, most values within this narrow interval providing equivalent results. The importance of well-tuned regularization to improve the quality of ASA and TDR maps is illustrated with a synthetic data set from Uieda et al. (2014), evaluated from adjacent bulk and linear magnetic sources. The efficiency of regularized derivatives is evaluated with aeromagnetic data showing a complex anomaly pattern with different directions and intersections, associated with shear zones, geologic faults, and intrusive bodies in the Proterozoic terrain of the Anápolis-Itauçu Complex (Della Giustina et al., 2011), situated in the Brasília Fold Belt central portion of Tocantins Province (Almeida et al., 1977, 1981), Brazil.

2. Methodology

This section initially describes common ASA and TDR transformed fields that employ first-order derivatives to enhance gridded magnetic data, to then introduce a simple criterion to determine a suitable regularization parameter better balancing noise amplification with smoothness constraint when evaluating regularized derivatives for a magnetic anomaly. Introduced by Nabighian (1984), the concept of the analytical signal amplitude for gridded data was formulated by Roest et al. (1992) as

$$|\mathbf{A}(x,y)| = \sqrt{\varphi_x^2 + \varphi_y^2 + \varphi_z^2}, \tag{1}$$

where $\varphi_x \equiv \varphi_x(x,y)$, $\varphi_y \equiv \varphi_y(x,y)$, and $\varphi_z \equiv \varphi_z(x,y)$ are the x, y, and z (vertical) first derivatives, respectively, of the magnetic field $\varphi(x,y)$ measured at positions (x,y) onto a plane at a constant flight height $z = h$. The importance in evaluating ASA for elongated anomalies is its symmetric bell-shaped signature (Macleod et al., 1993) over dike-like structures and geological contacts regardless the magnetization direction of the respective bodies, which simplifies the production of reliable geological maps. For three-dimensional bodies, ASA is sensitive to magnetization direction (Li, 2006) but still centered over the causative sources. The tilt derivative (TDR) represents the local phase of the analytical signal and is defined (Miller and Singh, 1994) as the ratio between the vertical and horizontal derivatives

$$\theta = \tan^{-1}\left[\frac{\varphi_z}{\sqrt{\varphi_x^2 + \varphi_y^2}}\right], \tag{2}$$

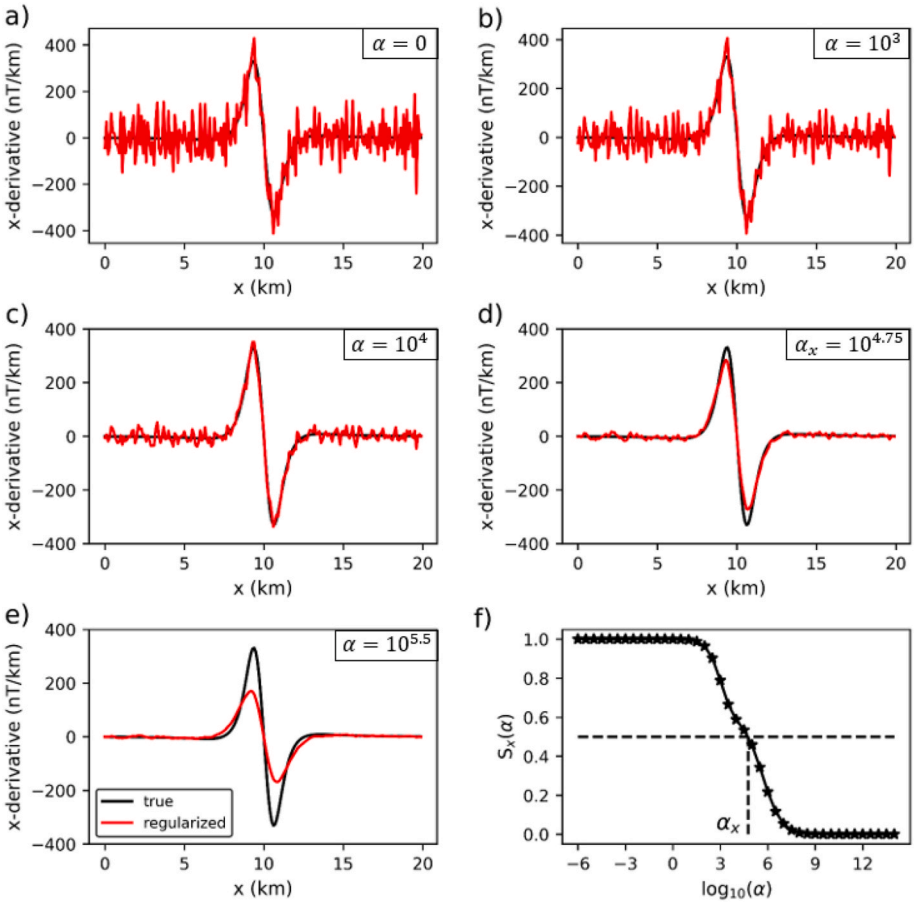

Fig. 3. S-function and associated first-order x-derivatives for different regularization parameters α: a) to e): true horizontal derivative (black line) and regularized horizontal derivative (red line) for a theoretical model without and with noise, respectively, and f) S-function with S = 0.5 reference (dashed line). The test values of the regularization parameter range from 10^{-6} to 10^{14} as a geometric progression with a ratio of $10^{0.5}$. The optimal value of the regularization parameter is equal to $\alpha_x = 10^{4.75}$, located on the half slope of the S-function. (For interpretation of the references to color in this figure legend, the reader is referred to the Web version of this article.)

for values in the interval of ± 90°. The TDR mapping is effective in normalizing the contributions from deep and shallow sources (Verduzco et al., 2004), thus equalizing the contributions from sources seated at different depth levels. The TDR usually shows null values at or near the edge of a vertical source with negative values at the flanks of the source region (Miller and Singh, 1994).

2.1. Regularized derivatives

The directional derivatives, φ_μ, for a magnetic field $\varphi(x,y)$, along a generic direction μ (often made as x, y, or z) can be obtained (Blakely, 1996, p. 324) in the Fourier domain, $\mathcal{F}\{\varphi_\mu\}$, by a simple filtering operation generically written as

$$\mathcal{F}\{\varphi_\mu\} = D_\mu \, \mathcal{F}\{\varphi\}, \tag{3}$$

for D_μ as ik_x, ik_y, and $|k| = \sqrt{k_x^2 + k_y^2}$ respectively for μ assigning directional derivatives along the x-, y-, and z-axes considering i the imaginary number, applied to the Fourier transformed anomaly, $\mathcal{F}\{\varphi\}$, regarding wavenumbers k_x and k_y along x- and y-directions. Once obtained in the Fourier domain, the derivative φ_μ is evaluated in the space domain by applying the inverse Fourier transform in the transformed field $\mathcal{F}\{\varphi_\mu\}$. In accordance with previous work on regularized derivatives (Pašteka et al., 2009; Gang and Lin, 2018), a general expression for the regularized filter, $D_{\mu,\alpha}$, for a given regularization parameter, α, can be written as

$$D_{\mu,\alpha} = \frac{D_\mu}{1 + \alpha B_\mu^2}, \tag{4}$$

with B_μ made as k_x, k_y, or $|k|$ respectively for μ assigning x-, y-, or z-derivative. The regularized μ-derivative in the Fourier domain, $\mathcal{F}\{\varphi_{\mu,\alpha}\}$, is evaluated as

$$\mathcal{F}\{\varphi_{\mu,\alpha}\} = D_{\mu,\alpha} \, \mathcal{F}\{\varphi\}, \tag{5}$$

making clear its dependence on a particular choice for the regularization parameter α. In the space domain, the regularized μ-derivative, $\varphi_{\mu,\alpha}$, is evaluated by applying the inverse Fourier transform to $\mathcal{F}\{\varphi_{\mu,\alpha}\}$. The regularized ASA and TDR are then obtained by using the regularized derivatives $\varphi_{x,\alpha}$, $\varphi_{y,\alpha}$, and $\varphi_{z,\alpha}$, in equations (1) and (2), respectively, instead of non-regularized derivatives φ_x, φ_y, and φ_z.

Fig. 1 illustrates how much the power spectrum of the regularized filter $D_{\mu,\alpha}$ departs from the respective non-regularized filter, regardless of the filter expression for derivatives along directions x, y or z. As α increases, the regularized filter gradually departs at higher wavenumbers to attenuate the higher wavenumber content of the transformed anomaly, meanwhile preserving its lower wavenumber content.

2.2. Regularization parameter criterion

The Tikhonov regularization parameter is a key parameter conditioning the smoothness degree of the unknown solution, weighting the additional constraints to guarantee that the obtained regularized solution is a well-suited approximation to the sought solution (Hansen, 1994). To determine a well-suited value for this parameter, we calculate the L_2-norm of first-order regularized derivatives, $\varphi_{\mu,\alpha}$, for trial α values in the range $[\alpha_l, \alpha_u]$. For a gridded data window with N_x and N_y data points along x and y-axes, the L_2-norm , $\| \bullet \|_2$, for the regularized derivative is evaluated as

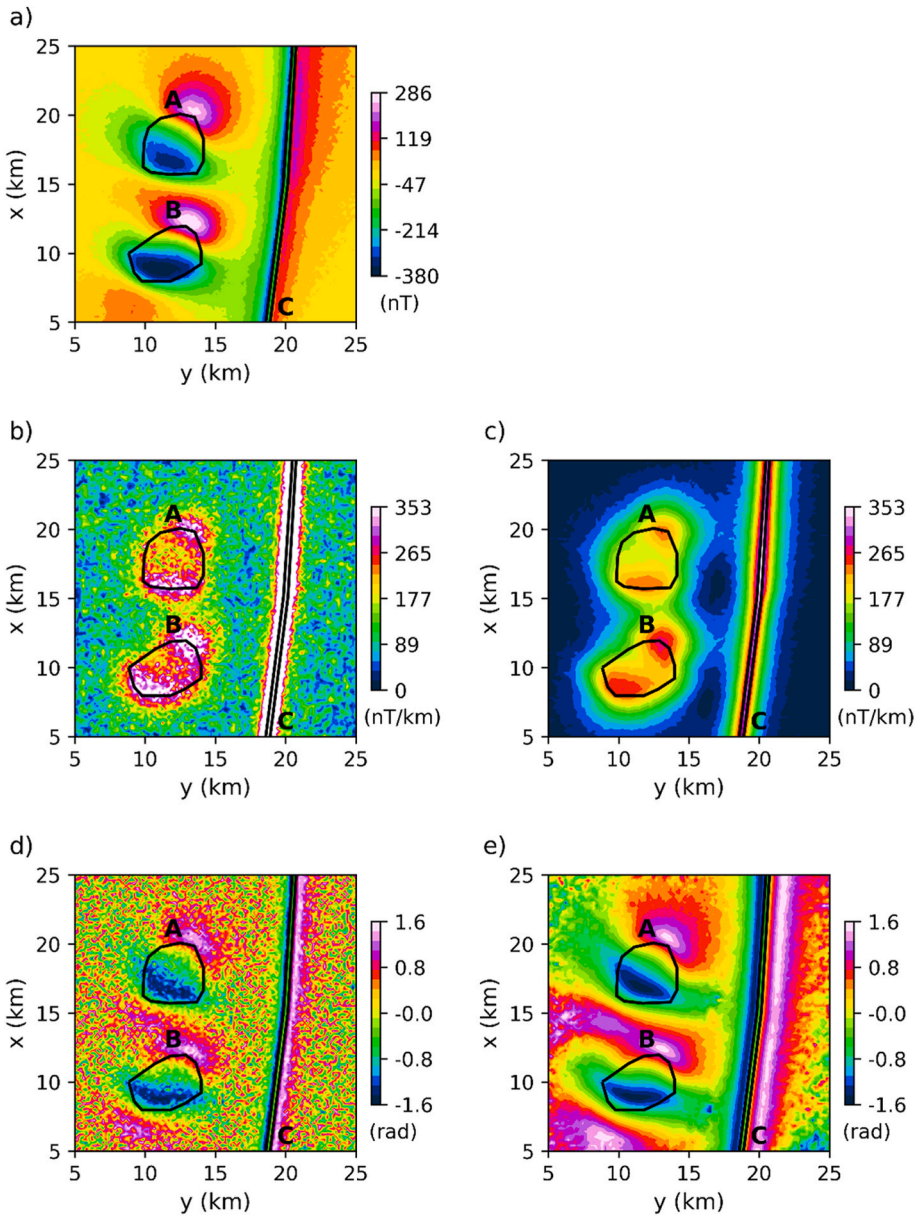

Fig. 4. Synthetic data and processed ASA and TDR maps: a) noise-corrupted total-field anomaly; analytical signal amplitude b) without and c) with regularization; tilt derivative d) without and e) with regularization for a model with three magnetic sources: batholith (A), sill (B), and dike (C). Magnetic anomaly considering a local main field with inclination and declination of -15° and 30°, respectively. Pseudo-random Gaussian noise with a mean of zero and a standard deviation of 5 nT is added to the calculated magnetic field. Sampling interval of 200 m.

$$\left\|\varphi_{\mu,\alpha}\right\|_2 = \sqrt{\sum_{j=0}^{N_y}\sum_{i=0}^{N_x}\left(\varphi_{\mu,\alpha}^{ij}\right)^2}, \tag{6}$$

where $\varphi_{\mu,\alpha}^{ij}$ is the regularized μ-derivative at the i,j-entry of the grid. The range $[\alpha_l, \alpha_u]$ must encompass several orders of magnitude, preferably with regular distribution in the logarithmic scale. The lower bound of the interval can be set to zero or to a very small number (10^{-6}, for example) to prevent numerical instabilities. In most cases, such a small number produces an equivalent result to the non-regularized condition with $\alpha = 0$. Due to unbounded noise amplification, the L_2-norm $\left\|\varphi_{\mu,0}\right\|_2$ (in this case assuming $\alpha_l = 0$) achieves its maximum value, monotonically decreasing as the trial α-values increase. As observed with synthetic and real data applications, the L_2-norm variation assumes a well-defined staircase shape, with marked flat stages at the ends (low and high α-values) of the interval on which the curve is defined. After normalization

$$S_\mu(\alpha) = \frac{\left\|\varphi_{\mu,\alpha}\right\|_2}{\left\|\varphi_{\mu,0}\right\|_2}, \tag{7}$$

This variation ranges from 1 to 0 (left to right) regardless of the choice for the directional derivative μ. Due to its general staircase shape, the function $S_\mu(\alpha)$ in equation (7) was termed as staircase function (S-function). An important feature of the S-function is its steep variation between the values at the end of the interval, which allows a simple way to locate the regularization parameter that preserves the signal amplitude, meanwhile preventing spurious oscillations for the evaluated field derivatives. In some cases, the S-function slope can be steeper, approaching the behaviour observed in the smoothed Heaviside function, where two steps are connected by a linear ramp changing sharply. When applied to a particular directional derivative, a set of S-functions $S_x(\alpha)$, $S_y(\alpha)$, and $S_z(\alpha)$ can be constructed, with the associated regularization parameters α_x, α_y, and α_z. As shown with synthetics and real data results, the regularization parameters at the S-function slope usually appear at a narrow interval within which similar x, y, and z smooth derivatives are obtained. The general behavior of a S-function is

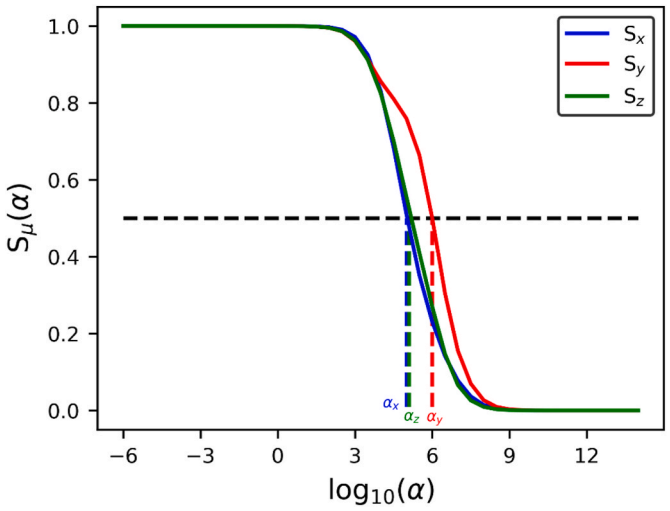

Fig. 5. S-function to μ-derivatives of the magnetic anomaly, where $\mu = (x,y,z)$. The test values of the regularization parameter range from 10^{-6} to 10^{14} as a geometric progression with a ratio of $10^{0.5}$. For each derivative, the optimal value of the regularization parameter is equal to $\alpha_x = 10^5$, $\alpha_y = 10^6$ and $\alpha_z = 10^{5.1}$, located on the half slope of the S-function.

illustrated in Fig. 2.

Fig. 3 illustrates how the amplitude filtered x-derivatives change for a set of trial regularization parameters according to their position in the S-function. The synthetic anomaly was evaluated from a tabular (two-dimensional) model composed of one prism at a top depth of 800 m, thickness of 1000 m, and induced magnetization of 3 A/m. The inclination and declination of the local main magnetic field are 90° and 0°, respectively. The magnetic anomaly was calculated at a flight height of 100 m then corrupted with zero-mean, 5 nT pseudorandom Gaussian noise. We evaluate the x-derivatives of the magnetic anomaly without and with noise in Fig. 3. The well-behaved shape of the S-function is shown in Fig. 3f, its two ends of the interval are connected by a steep slope. The non-regularized derivative ($\alpha = 0$) in Fig. 3a gives the most oscillating derivative, gradually getting smoother derivatives for $\alpha = 10^3$ and $\alpha = 10^4$ (Figs. 3b and c) which corresponds to a variation from 1 to near 0.4 in the S-function. In each case, the difference between filtered and model-evaluated derivatives can be compared, this difference increasing as the regularization parameter is set at higher values. As α reaches $10^{5.5}$ (Fig. 3e), the curve of the regularized derivative loses about half of its amplitude, a typical condition of an over-regularized case. The choice $\alpha_x = 10^{4.75}$ (Fig. 3d) corresponding to the L_2-norm equal to 0.5 gives in this example the best result, either preserving the amplitude of the filtered derivative as well as cleaning oscillations from noise amplification (Fig. 3f). Note that even in this case the regularized derivative does not perfectly reproduce the true derivative (evaluated directly from the model) since a loss in amplitude still is presented (Fig. 3d).

In processing a gridded data set to obtain regularized ASA and TDR maps, the S-function must be constructed for each of the x, y, and z directional derivatives thus obtaining S_x, S_y, and S_z curves. The condition $S_{x,y,z} = 0.5$ is established to define corresponding α_x, α_y, and α_z regularization parameters. To obtain a single regularization parameter, α_g, representing the mean value of α_x, α_y, and α_z in the log-scale, we can use

$$\alpha_g = 10^{\left(\tilde{\alpha}_x+\tilde{\alpha}_y+\tilde{\alpha}_z\right)/3}, \tag{8}$$

where $\tilde{\alpha}_\mu \equiv \log_{10}\alpha_\mu$ assuming μ equivalent to x-, y-, or z-derivatives. The α_g can be used to evaluate the derivatives related to ASA and TDR computation, in this case using a single regularization parameter for all derivatives. The steep slope of the S-curves in all cases makes this mean parameter close to the previous ones, thus providing equivalent results as obtained with α_x, α_y, and α_z. The half-slope condition $S_{x,y,z}(\alpha_{x,y,z}) = 0.5$ has proved useful in most synthetics and real data applications with ASA and TDR evaluations. Depending on the noise level in the data, a lower ($S_{x,y,z} > 0.5$) or higher ($S_{x,y,z} < 0.5$) regularization degree can be applied in order to obtain ASA and TDR maps that best enhance the continuity of magnetic lineaments and general trends.

3. Computational implementation

The evaluation of the regularization procedure to synthetic and real data was implemented in Python using the routines "synthetic_data.py" and "real_data.py", respectively. The auxiliary program "filtering.py" evaluates the directional non-regularized derivatives in the Fourier domain (equation (3)) by function "nonregularized_derivative". This function uses a similar structure to the functions of the "Fatiando a Terra" version 0.5 package (fatiando.org) that computes the non-regularized derivatives by the central finite-differences method or by the Fast Fourier Transform. The function "regularized_derivative" implements the regularized derivatives in the Fourier domain as shown in equation (5). To construct the S-function, the normalized L_2-norm of the derivatives (equation (7)) for a set of trial regularization parameters is evaluated in the function "s_function" in the program "filtering.py". As the S-function is evaluated for regularization parameter discrete values, we use Python's sklearn module to fit a linear approximation of the S-function slope portion to determine the well-suited regularization parameters. The conventional (non-regularized) and regularized ASA (equation (1)) and TDR (equation (2)) are evaluated by function "asa_tdr" after the calculation of the directional derivatives. The outputs of the non-regularized and regularized ASA and TDR in the script "real_data.py" can be exported in a file with xyz-extension to the software Oasis Montaj (tested with v. 8.4) to reproduce the maps in different color scales. The Python program also generates corresponding figures, but their color scale does not clearly illustrate subtle magnetic lineaments or general trends. In the Oasis Montaj, the magnetic anomaly, ASA, and TDR were interpolated by the minimum curvature method with a cell size of 125 m to generate the grids, and next integrated to geological databases with QGIS v. 3.12.1.

4. Numerical simulation

The synthetic data set to evaluate the regularization procedure presented in this section is illustrated with synthetics made available by Uieda et al. (2014) at http://github.com/pinga-lab/paper-tle-euler-tutorial, and included in the folder with programs. The magnetic model that generated this synthetic gridded data set is composed of three prismatic bodies with induced magnetization: a bulk-prism simulating a batholith with a magnetization of 2 A/m at a top depth of 500 m; a plate-like prism simulating a sill with a magnetization of 10 A/m with the top at the depth of 1000 m and an elongated prism simulating a dike located at the ground surface (depth at z = 0), 300 m mean-wide, and magnetization of 10 A/m (Fig. 4). The inclination and declination of the local main magnetic field are −15° and 30°, respectively. The magnetic field calculated at a flight height of 300 m contains 5 nT of pseudo-random Gaussian noise.

Fig. 4 shows output ASA and TDR maps from conventional and regularized procedures as applied to noisy synthetic data with sampling interval of 200 m (Fig. 4a). Both maps of ASA (Fig. 4b) and TDR (Fig. 4d) without regularization show artifacts associated with noise amplification that prevents a clear positioning of the ASA peaks at the edges of the sources (Fig. 4b). The regularized ASA and TDR maps were evaluated with regularized x-, y-, and z-derivatives with $\alpha_g = 10^{5.4}$, computed by equation (8), considering α_x, α_y, and α_z respectively equal to 10^5, 10^6 and $10^{5.1}$ (Fig. 5). As shown in Fig. 5, these regularization parameters

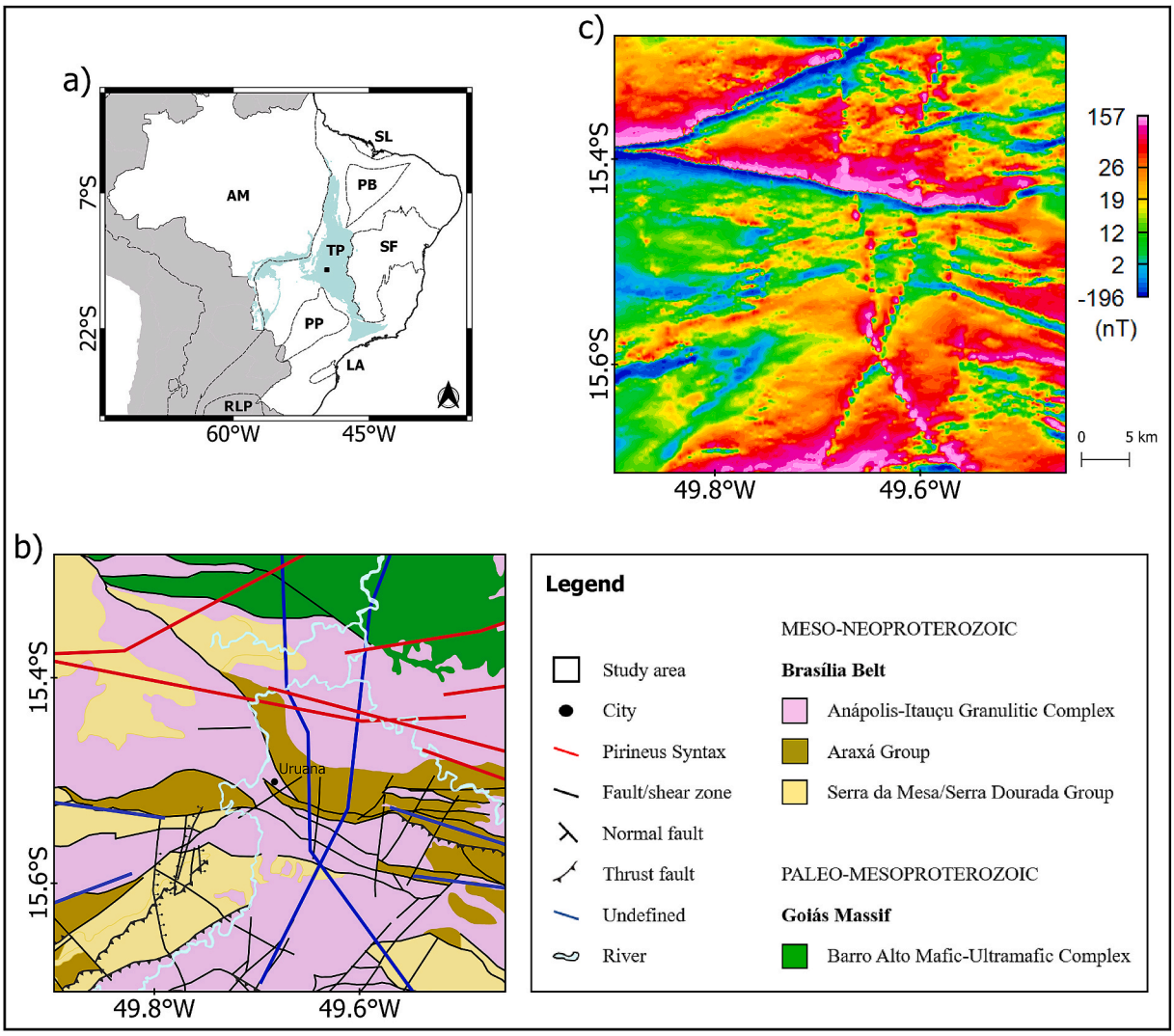

Fig. 6. a) Study area (black polygon) at the Brasília Fold Belt central portion in the Tocantins Province (TP). b) Schematic geological map for the study area based on the shape file from the Brazil Geological Survey, available at "http://www.sieg.go.gov.br/siegdownloads/". c) Magnetic anomaly map. Cratons: São Francisco (SF), Paranapanema (PP), São Luis (SL), Rio de La Plata (RLP), Amazônico (AM), Luiz Alves (LA), and Parnaíba (PB).

are close to the S-function value equal to 0.5, thus enforcing an appropriate smoothness degree to provide ASA (Fig. 4c) and TDR (Fig. 4e) maps with lower distortions from noise amplification. As in Fig. 4c, the peaks of the regularized ASA are better positioned over the edges of the bulky bodies and the center of the elongated prism as well, better outlining the distribution of the prismatic magnetic sources. The regularized TDR in Fig. 4e enhances the signal changes at the edges, better defining the negative portion of the elongated anomaly than conventional TDR (Fig. 4d). In Fig. 4e, the extension where TDR shows positive variations increased, extrapolating toward the ends of the grid due to border effects. The $S = 0.5$ criterion adopted in this test qualitatively guarantees that most of the spurious features at the output maps were removed. In replicating this test for $S = 0.75$ for example, a still noisy result close to the conventional output is observed, suggesting a milder regularization degree under such a condition. An important contribution of the proposed approach is producing graphical support showing that close regularization parameters can be set for all directional derivatives, their respective S-curves informing how much amplitude loss was required to obtain reliable ASA and TDR maps keeping the continuity of lineaments and outlining the boundaries of bulky bodies.

5. Real data application

The proposed procedure is applied to aeromagnetic data covering the Anápolis-Itauçu Complex north limit, situated in the Brasília Fold Belt central portion, in the Neoproterozoic Tocantins Province (Fig. 6a). Anápolis-Itauçu Complex, an exposed metamorphic core of the Brasília Belt, is composed of high-grade metamorphic rocks (orthogneisses, amphibolites, metasediments, among others) and ultrahigh temperature granulite that has been dated with zircon ages varying between 760 and 650 Ma (Della Giustina et al., 2011). East of the study area, the Pirineus Zone of High Strain (D'el-Rey Silva et al., 2011) or Pirineus Syntax (Araújo Filho, 2000) may have deformed the study area terrains. Pirineus Syntax is a dextral transcurrent shear megazone with about 300 km long (D'el-Rey Silva et al., 2011), composed of a set of E-W and WNW-ESE structural lineaments, marking the geotectonic structural limit between the north and south segments of the Brasília Belt (Araújo Filho, 2000). This shear zone presents syntax curvature facing east, associated with terrain accretion to the Craton São Francisco western margin (Filgueiras, 2015). According to Araújo Filho and Kuyumjian (1996) and Araújo Filho (2000), the PS's origin is interpreted as a polyphasic collision comprising deformations WSW to ENE, NNW to SSE and WSW to ENE. Several extensive NW and NE-oriented strip-slip faults

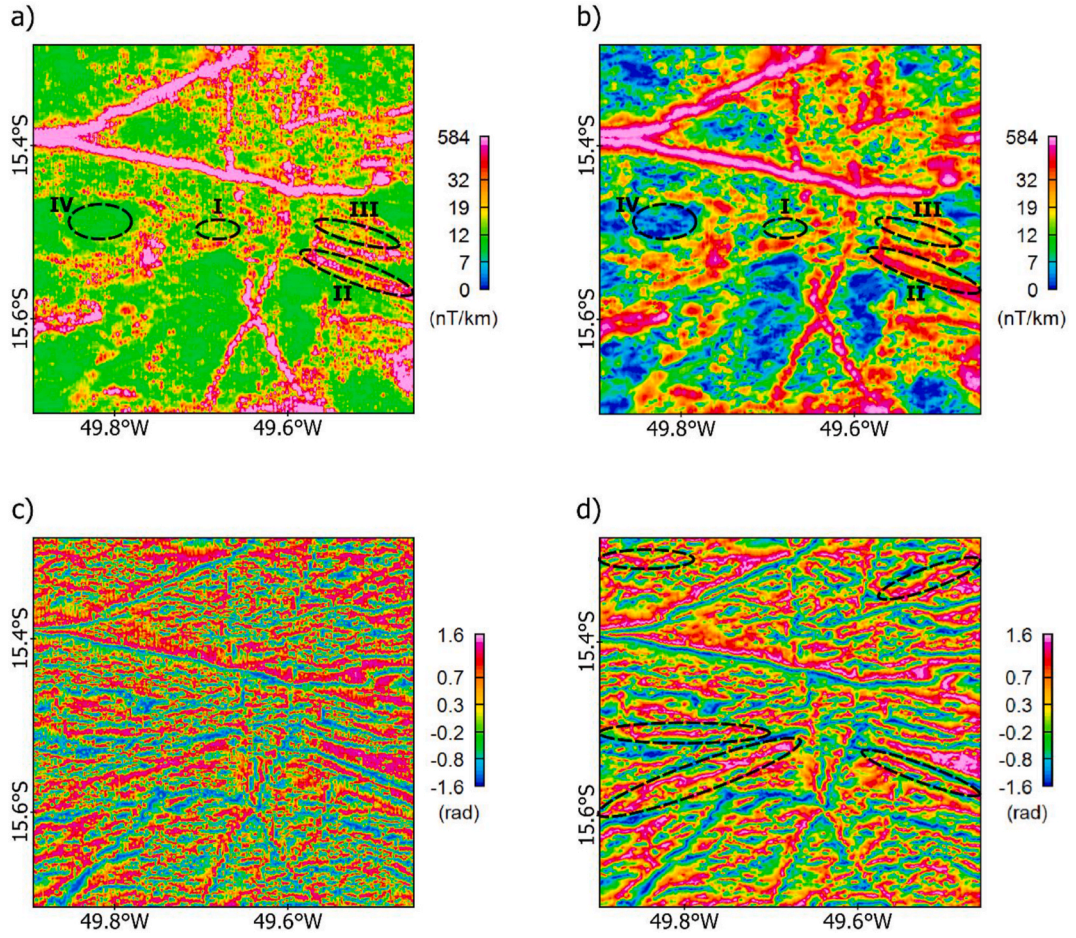

Fig. 7. Conventional and regularized maps: analytical signal amplitude a) without and b) with regularization; tilt derivative c) without and d) with regularization. Key features (black dashed line) discussed in the text, in terms of flight line distortion (I), "boudinage" effects (II), continuity and amplitude gain of the lineaments (III), and low amplitude anomalies (IV). In map d), W-E, ESE-WNW, and WSW-ENE lineaments (black dashed line).

possibly generated in the late phase of the Brasiliano Cycle (Araújo Filho, 2000; Martins-Ferreira and Rodrigues, 2021), and syn- and post-collisional granitic bodies intrude along this high ductile deformation zone (Pimentel et al., 2003; Sandoval, 2016; Silva, 2018; Martins-Ferreira and Rodrigues, 2021). The PS is located between the layered mafic-ultramafic intrusions of the Barro Alto Complex and the high-grade metamorphic rocks from the Anápolis-Itauçu Complex, surrounded by low-grade metasedimentary successions from the Araxá and Serra da Mesa/Serra Dourada groups (Pimentel et al., 1999; 2000, 2011) (Fig. 6b). Granulitic mafic-ultramafic intrusions and deformed syn-tectonic granitic intrusions aged between 660 and 650 Ma (Piuzana et al., 2003) emplaced into deep-crustal levels occur in the Anápolis-Itauçu Complex and in the Araxá and Serra da Mesa/Serra Dourada groups, forming NW-SE elongated bodies with varied dimensions (Pimentel et al., 1999; 2000; Della Giustina et al., 2011). The geological units of the study area (Fig. 6b) are tectonically limited by thrust faults, low- and high-angle shear zones, and normal and reverse faults, associated with deformational processes and terrain accretions in the Brasília Belt in the final stage of the Brasiliano orogeny (Almeida et al., 1981; Fonseca et al., 1995; Pimentel et al., 1999; 2011; Piuzana et al., 2003; Valeriano et al., 2008; Uhlein et al., 2012; Pimentel, 2016).

The aeromagnetic data covering this region was acquired by the Brazil Geological Survey– CPRM in 2005, along North-South flight lines 500 m apart, tie lines at a pace of 5000 m, at the uniform barometric height of 100 m above the ground surface (Prospecções, 2006). The local geomagnetic field for the date of the survey has mean intensity of 23,856 nT, inclination of −20.84°, and declination of −19.21°. The acquired data was micro-levelled (Minty, 1991) by Lasa Engenharia e Prospecções S/A, and the entire database with code 3013 can be requested for academic purposes from the State of Goiás Division for Geology and Mining Affairs. The total-field anomaly (Fig. 6c) was interpolated by the minimum curvature method (Santos et al., 2016) with cell size of 125 m (1/4 of the spacing of the flight lines). The main magnetic features observed in the anomaly map are lineaments with different orientations (WSW-ENE, ESE-WNW, SSE-NNW, SSW-NNE). Most anomalies show normal polarity patterns, indicative of predominantly induced magnetization (Fig. 6c). The survey area shows multiple intersections of lineaments and interrupted features along specific lineaments (Fig. 6c), making it well-suited to evaluate procedures looking for lineament enhancement and interpretation.

In Figs. 7 and 8, the same transformed fields are illustrated, only with different colour scales. The ASA without regularization embodies spurious effects in the N–S flight lines and discontinuous "boudins" along linear features (Figs. 7a–8a). Crenulations associated with the N–S flight lines also appear in the TDR map without regularization (Figs. 7c–8c). The regularized ASA and TDR maps were evaluated with regularized x-, y-, and z-derivatives with $\alpha_g = 10^{4.5}$, computed by equation (8), considering α_x, α_y, and α_z respectively equal to $10^{4.6}$, $10^{4.5}$ and $10^{4.5}$ (Fig. 9). In Figs. 7b–8b, the regularized ASA better tracks the continuity of the lineaments by attenuating the "boudinage" effect, enhancing the amplitude, and better defining their ends, meanwhile partially removes the N–S artifacts associated with the flight line direction. As shown in Fig. 7b, there are low amplitude anomalies (between 0 and 7 nT/km) distributed in several regions of the regularized ASA map, working as

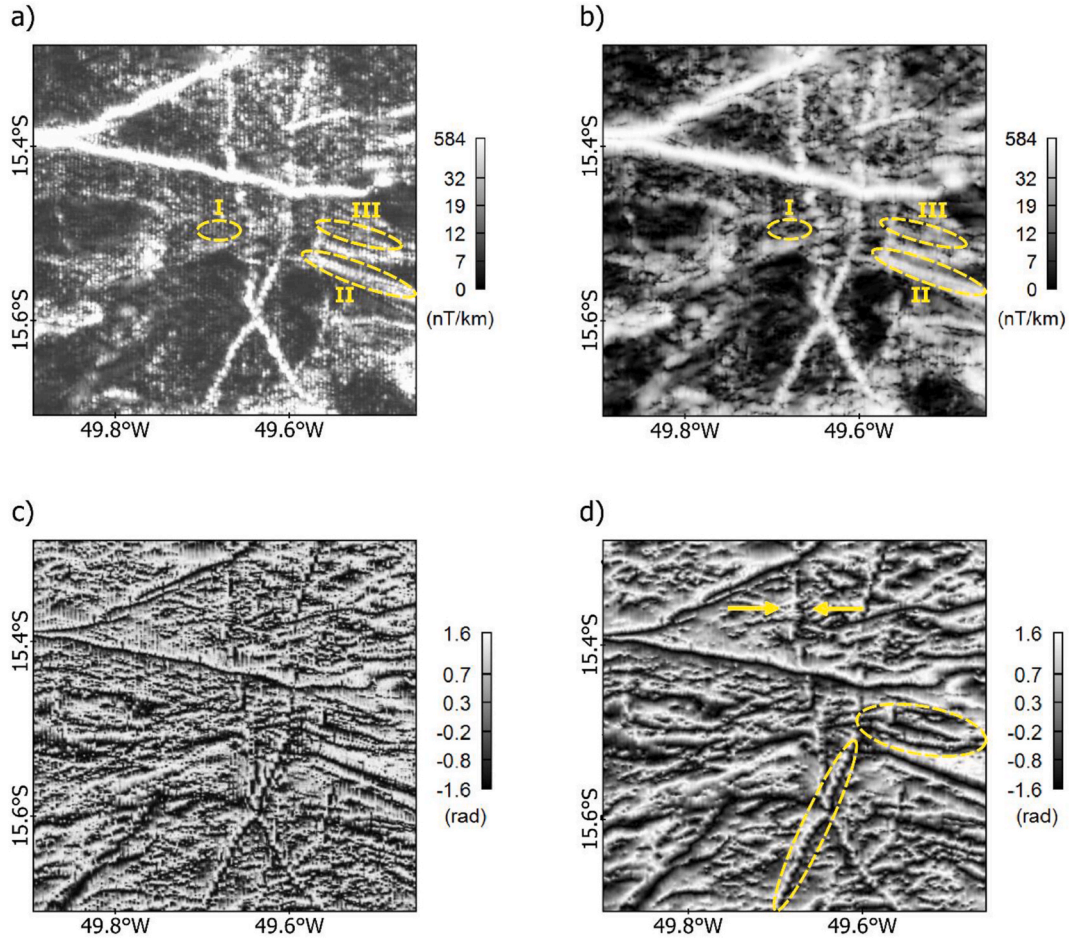

Fig. 8. Conventional and regularized maps: analytical signal amplitude a) without and b) with regularization; tilt derivative c) without and d) with regularization. Key features (yellow dashed line) discussed in the text, in terms of flight line distortion (I), "boudinage" effects (II), and continuity and amplitude gain of the lineaments (III). In map d), dislocated lineaments (yellow arrows) and continuous features (yellow dashed line). (For interpretation of the references to color in this figure legend, the reader is referred to the Web version of this article.)

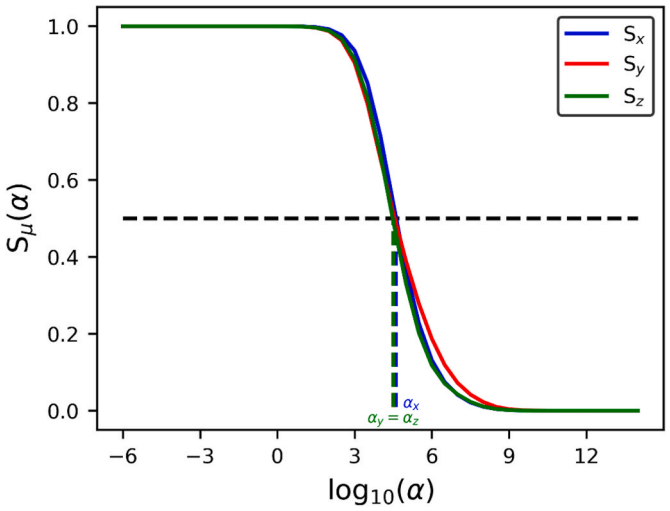

Fig. 9. S-function to μ-derivatives of the magnetic anomaly, where $\mu = (x,y,z)$. The test values of the regularization parameter range from 10^{-6} to 10^{14} as a geometric progression with a ratio of $10^{0.5}$. For each derivative, the optimal value of the regularization parameter is equal to $\alpha_x = 10^{4.6}$ and $\alpha_y = \alpha_z = 10^{4.5}$, located on the half slope of the S-function.

magnetic source separators. The regularized TDR in Fig. 7d attenuates the crenulations associated with the flight line direction, mapping W-E, ESE-WNW, and WSW-ENE lineaments that are not observed in the regularized ASA (Fig. 7b), better defining the edges of the lineaments. As in Fig. 8d, the regularized TDR map highlights the lateral displacement of north-south lineaments and the continuity of some linear features in the intersections. The direction of the magnetic lineaments mapped by the ASA and TDR (Figs. 7 and 8) coincides with the Pirineus Syntax's E-W and WNW-ESE structural lineaments, fault/shear zones, possible Neoproterozoic NW-SE granitic and mafic-ultramafic intrusions, and NW and NE-oriented strip-slip faults (Fig. 6b). This complex structural framework was generated during the continental collision of the Amazon, São Francisco, and Paranapanema cratons in the Brasiliano Cycle final stage.

6. Conclusions

The procedure to estimate the proper regularization parameter based on the graphical construction of a characteristic staircase function associated with the L_2-norm of the regularized derivative shows efficiency in improving the quality of processed aeromagnetic data. The analysis of the S-function for a given directional derivative informs how much amplitude loss is required to obtain reliable, no over-smoothed transformed fields. The half-slope condition shows effectiveness for the tested synthetic and real data sets. However, depending on the noise level in the data, a lower or higher regularization degree can be

experimented to try a better tuning between noise amplification and amplitude loss. General aspects of the processed products in terms of the continuity of lineaments or in recovering known geological trends may justify the shift of the S-function from its half-slope condition. For the tested real data set, the regularized versions for ASA and TDR attenuate artifacts associated with "boudinage" and flight line distortions, enhancing the continuity of the linear features, the intersections of distinct magnetic trends, the expression of weakly magnetic structures, and in general, better recognizing the extension of intercepting magnetic lineaments. The magnetic features identified by ASA and TDR coincide with the Pirineus Syntax's structural lineaments, fault/shear zones, and possible Neoproterozoic NW-SE granitic and mafic-ultramafic intrusions. This result indicates the Pirineus Zone of High Strain may have affected a larger area than previously studied by other authors.

Computer code availability section

Name of the code/library: Staircase_Function Contact: janaina.melo@usp.br; (13)996202131, Program language: Python.

Software required: IDE Python.

Programs mean size: 5 – 15 KB.

The source codes are available for downloading at the link: https://github.com/janainaanjos/Staircase_Function.

CRediT authorship contribution statement

Janaína Anjos Melo: Writing – review & editing, Writing – original draft, Software, Methodology, Formal analysis, Data curation, Conceptualization. **Carlos Alberto Mendonça:** Writing – review & editing, Writing – original draft, Supervision, Project administration, Methodology, Formal analysis, Conceptualization. **Yara Regina Marangoni:** Writing – review & editing, Writing – original draft, Visualization, Formal analysis.

Declaration of competing interest

The authors declare that they have no known competing financial interests or personal relationships that could have appeared to influence the work reported in this paper.

Data availability

I have shared the link to my code at the Attach File step

Acknowledgments

This work was in part funded by FAPESP 2019/20172–7 and the Coordenação de Aperfeiçoamento de Pessoal de Nível Superior - Brasil (CAPES) - Finance Code 001".

References

Almeida, F.F.M., Hasui, Y., Brito Neves, B.B., Fuck, R.A., 1977. Províncias estruturais brasileiras. In: Simpósio de Geologia do Nordeste, vol. 8, pp. 363–391.

Almeida, F.F.M., Hasui, Y., Brito Neves, B.B., Fuck, R.A., 1981. Brazilian structural provinces: an introduction. Earth Sci. Rev. 17 (1–2), 1–29. https://doi.org/10.1016/0012-8252(81)90003-9.

Araújo Filho, J.O., 2000. The Pirineus syntaxis: an example of intersection of two Brasiliano fold-thrust belts in Central Brazil, and its implications for the tectonic evolution of Western Gondwana. Rev. Bras. Geociencias. 30 (1), 144–148.

Araújo Filho, J.O., Kuyumjian, R.M., 1996. Regional distribution and structural control of the gold occurrences/deposits in the Goiás Massif and Brasília Belt. Braz. J. Genet. 26 (2), 109–112.

Aster, R.C., Borchers, B., Thurber, C.H., 2013. Parameter Estimation and Inverse Problems, second ed. Academic Press, p. 377.

Blakely, R.J., 1996. Potential Theory in Gravity and Magnetic Applications, second ed. Cambridge University Press, p. 461.

Cooper, G.R.J., 2014. Reducing the dependence of the analytic signal amplitude of aeromagnetic data on the source vector direction. Geophysics 79 (4). https://doi.org/10.1190/geo2013-0319.1. J55–J60.

Cooper, G.R.J., Cowan, D.R., 2006. Enhancing potential field data using filters based on the local phase. Comput. Geosci. 32 (10), 1585–1591. https://doi.org/10.1016/j.cageo.2006.02.016.

Della Giustina, M.E.S., Pimentel, M.M., Ferreira Filho, C.F., Hollanda, M.H.B.M., 2011. Dating coeval mafic magmatism and ultrahigh temperature metamorphism in the Anápolis–Itauçu Complex, Central Brazil. Lithos 124 (1–2), 82–102. https://doi.org/10.1016/j.lithos.2010.11.004.

D'el-Rey Silva, L.J.H., Oliveira, Í.L., Pohren, C.B., Tanizaki, M.L.N., Carneiro, R.C., Fernandes, G.L.F., Aragão, P.E., 2011. Coeval perpendicular shortenings in the Brasília belt: collision of irregular plate margins leading to oroclinal bending in the Neoproterozoic of central Brazil. J. S. Am. Earth Sci. 32 (1), 1–13. https://doi.org/10.1016/j.jsames.2011.02.013.

Ferreira, F.J.F., Souza, J., Bongiolo, A.B.S., Castro, L.G., 2013. Enhancement of the total horizontal gradient of magnetic anomalies using the tilt angle. Geophysics 78 (3), J33–J41. https://doi.org/10.1190/geo2011-0441.1.

Filgueiras, B.D.C., 2015. Depósito Vulcanogênico Polimetálico (Zn, Pb, Cu±(Ag-Bi)) Artulândia, Arco Magmático Paleoproterozóico Campinorte, Brasil Central. Dissertação de Mestrado. Universidade de Brasília, Instituto de Geociências, Brasília, p. 122.

Fonseca, M.A., Dardenne, M.A., Uhlein, A., 1995. Faixa Brasília setor setentrional: estilos estruturais e arcabouço tectônico. Rev. Bras. Geociencias. 25 (4), 267–278.

Gang, Y., Lin, Z., 2018. An improved stable downward continuation of potential fields using a truncated Taylor series and regularized vertical derivatives method. J. Geophys. Eng. 15 (5), 2001–2008. https://doi.org/10.1088/1742-2140/aac53a.

Hansen, P.C., 1994. Regularization tools: a Matlab package for analysis and solution of discrete ill-posed problems. Numer. Algorithm. 6 (1), 1–35. https://doi.org/10.1007/BF02149761.

Hansen, P.C., 1998. Rank-deficient and Discrete Ill-Posed Problems: Numerical Aspects of Linear Inversion, first ed. Society for Industrial and Applied Mathematics, p. 263.

Li, X., 2006. Understanding 3D analytic signal amplitude. Geophysics 71 (2), L13–L16. https://doi.org/10.1190/1.2184367.

Ma, G., Liu, C., Li, L., 2014. Balanced horizontal derivative of potential field data to recognize the edges and estimate location parameters of the source. J. Appl. Geophys. 108, 12–18. https://doi.org/10.1016/j.jappgeo.2014.06.005.

MacLeod, I.N., Jones, K., Dai, T.F., 1993. 3-D analytic signal in the interpretation of total magnetic field data at low magnetic latitudes. Explor. Geophys. 24 (4), 679–688. https://doi.org/10.1071/EG993679.

Martins-Ferreira, M.A.C., Rodrigues, S.W.D.O., 2021. Field guide to RODS in the pireneus syntaxis, central Brazil. In: Structural Geology and Tectonics Field Guidebook—Volume 1, pp. 221–264.

Miller, H.G., Singh, V., 1994. Potential field tilt - a new concept for location of potential field sources. J. Appl. Geophys. 32 (2–3), 213–217. https://doi.org/10.1016/0926-9851(94)90022-1.

Minty, B.R.S., 1991. Simple micro-levelling for aeromagnetic data. Explor. Geophys. 22 (4), 591–592. https://doi.org/10.1071/EG991591.

Morozov, V.A., 1966. On the solution of functional equations by the method of regularization. Dokl. Akad. Nauk. SSSR. 167 (3), 510–512.

Nabighian, M.N., 1984. Toward a three-dimensional automatic interpretation of potential field data via generalized Hilbert transforms: fundamental relations. Geophysics 49 (6), 780–786. https://doi.org/10.1190/1.1441706.

Pašteka, R., Richter, P., 2002. A simple approach to regularized gradients calculation in gravimetry and magnetometry. In: 64th EAGE Conference & Exhibition. European Association of Geoscientists & Engineers cp–5.

Pašteka, R., Richter, F.P., Karcol, R., Brazda, K., Hajach, M., 2009. Regularized derivatives of potential fields and their role in semi-automated interpretation methods. Geophys. Prospect. 57 (4), 507–516. https://doi.org/10.1111/j.1365-2478.2008.00780.x.

Pham, L.T., Oksum, E., Do, T.D., Le-Huy, M., Vu, M.D., Nguyen, V.D., 2019. LAS: a combination of the analytic signal amplitude and the generalized logistic function as a novel edge enhancement of magnetic data. Contrib. Geophys. Geodes. 49 (4), 425–440. https://doi.org/10.2478/congeo-2019-0022.

Pimentel, M.M., 2016. The tectonic evolution of the Neoproterozoic Brasília Belt, central Brazil: a geochronological and isotopic approach. Braz. J. Genet. 46, 67–82.

Pimentel, M.M., Fuck, R.A., Fischel, D.P., 1999. Estudo isotópico Sm-Nd regional da porção central da Faixa Brasília: implicações para a idade e origem dos granulitos do Complexo Anápolis-Itauçu e sedimentos do Grupo Araxá. Braz. J. Genet. 29 (2), 271–276.

Pimentel, M.M., Fuck, R.A., Jost, H., Ferreira Filho, C.F., Araújo, S.M., 2000. The basement of the Brasília fold belt and the Goiás magmatic arc. Tectonic Evolution of South America 31, 195–229.

Pimentel, M.M., Dantas, E.L., Fuck, R.A., Armstrong, R.A., 2003. Shrimp and conventional U-Pb age, Sm-Nd isotopic characteristics and tectonic significance of the K-rich Itapuranga suite in Goiás, central Brazil. An Acad. Bras Ciências. 75, 97–108.

Pimentel, M.M., Rodrigues, J.B., Della Giustina, M.E.S., Junges, S., Matteini, M., Armstrong, R., 2011. The tectonic evolution of the Neoproterozoic Brasília Belt, central Brazil, based on SHRIMP and LA-ICPMS U–Pb sedimentary provenance data: a review. J. S. Am. Earth Sci. 31 (4), 345–357. https://doi.org/10.1016/j.jsames.2011.02.011.

Piuzana, D., Pimentel, M.M., Fuck, R.A., Armstrong, R., 2003. Neoproterozoic granulite facies metamorphism and coeval granitic magmatism in the Brasilia Belt, Central Brazil: regional implications of new SHRIMP U–Pb and Sm–Nd data. Precambrian Res. 125 (3–4), 245–273. https://doi.org/10.1016/S0301-9268(03)00108-6.

Richter, P., Pašteka, R., 2003. Influence of norms on calculation of regularized derivatives in geophysics. Contrib. Geophys. Geodes. 33 (1), 1–16.

Roest, W.R., Verhoef, J., Pilkington, M., 1992. Magnetic interpretation using the 3-D analytic signal. Geophysics 57 (1), 116–125. https://doi.org/10.1190/1.1443174.

Sandoval, S.A.R., 2016. Caraterização petrográfica, geoquímica e isotópica do sienito de Uruana e suas implicações sobre a gênese do magmatismo sin-tectônico da Faixa Brasília. Dissertação de Mestrado. Universidade de Brasília, Instituto de Geociências, Brasília, p. 96.

Santos, H.S., Cunha, G.N., Castro, J.R., 2016. Avaliação qualitativa das técnicas de interpolação de mínima curvatura, krigagem e bidirecional na formação de imagens. Revista de Engenharias da Faculdade Salesiana (4), 2–16.

Silva, A.C.V.R., 2018. Caraterização petrográfica, geoquímica e isotópica do Granito Itapuranga na porção central da Faixa Brasília. Dissertação de Mestrado. Universidade de Brasília, Instituto de Geociências, Brasília, p. 82.

Tikhonov, A.N., Glasko, V.B., 1965. Application of the regularization method in nonlinear problems. J. Comp. Math. Math. Phys. 5 (3), 363–373.

Uhlein, A., Fonseca, M.A., Seer, H.J., Dardenne, M.A., 2012. Tectônica da faixa de dobramentos Brasília-setores setentrional e meridional. Geonomos 20 (2), 1–14.

Uieda, L., Oliveira Jr., V.C., Barbosa, V.C.F., 2014. Geophysical tutorial: euler deconvolution of potential-field data. Lead. Edge. 33 (4), 448–450. https://doi.org/10.1190/tle33040448.1.

Valeriano, C.M., Pimentel, M.M., Heilbron, M., Almeida, J.C.H., Trouw, R.A.J., 2008. Tectonic evolution of the Brasília belt, Central Brazil, and early assembly of gondwana. Geol. Soc. Lond. Spec. Publ. 294 (1), 197–210. https://doi.org/10.1144/SP294.11.

Verduzco, B., Fairhead, J.D., Green, C.M., MacKenzie, C., 2004. New insights into magnetic derivatives for structural mapping. Lead. Edge 23 (2), 116–119. https://doi.org/10.1190/1.1651454.

Wijns, C., Perez, C., Kowalczyk, P., 2005. Theta map: edge detection in magnetic data. Geophysics 70 (4), 39–43. https://doi.org/10.1190/1.1988184.

Zhang, X., Yu, P., Tang, R., Xiang, Y., Zhao, C.J., 2014. Edge enhancement of potential field data using an enhanced tilt angle. Explor. Geophys. 46 (3), 276–283. https://doi.org/10.1071/EG13104.

Prospecções, L.A., 2006. Relatório Final do Levantamento e Processamento dos Dados Magnetométricos e Gamaespectométricos – Levantamento Aerogeofísico do Estado de Goiás – 3ª Etapa. Texto técnico. Convênio SGM/MME/CPRM – SIC/SGM/FUNMINERAL, p. 138.